Experimental Verification of Inelastic Design Procedures for Steel Bridges

Michael G. Barker and Bryan A. Hartnagel, *University of Missouri, Columbia*

The first of three composite girder tests is presented from a project with the objectives of validating current inelastic design procedures and developing new inelastic provisions for bridges comprising noncompact girders. The first girder test was a half-scale, three-span composite beam with compact sections. The future tests will be two-span composite girders comprising noncompact sections. The essential components of inelastic design provisions are moment-inelastic rotation relations at the critical sections. These relations are necessary to predict inelastic rotations, permanent residual deflections, and redistributed moments in the structure. Along with the design and modeling of the half-scale test, experimental moment-rotation behavior characteristics for moving load inelastic tests and a plastic collapse test are presented. Inelastic behavior in terms of design limits and predicting residual deformations is presented on the basis of the experimental results.

Inelastic steel bridge design procedures account for the reserve strength inherent in multiple-span steel girder bridges by allowing redistribution of negative pier region elastic moments to adjacent positive moment regions (*1*,*2*). The redistribution causes slight inelastic rotation at the interior pier sections, residual moments in the beam, and some permanent residual deflection. After the redistribution, the structure achieves shakedown (*3*,*4*): deformations stabilize and future loads are resisted elastically.

The AASHTO Alternate Load Factor Design (ALFD) (*1*) method allows inelastic design for bridges comprising compact sections. ALFD is incorporated into the AASHTO Load and Resistance Factor Design (LRFD) Bridge Design Specification (*2*). Inelastic design procedures allow the designer flexibility and the possibility of more economical designs by eliminating cover plates and flange transitions at negative moment regions (*5*). Expanding inelastic designer provisions to include noncompact sections is desirable because of the wide use of plate girders with thin webs.

This paper presents results of a ½-scale composite girder test. In all, three composite girders, each approximately 30.5 m (100 ft) long, will be tested. Simulated moving loads in the elastic and inelastic range will be cyclically applied to the test girders. Afterward, the girders will be tested to failure in a static collapse configuration. The first test consists of a three-span, compact, rolled section, whereas the other two will be two-span girders with typical noncompact plate girder sections. The project will verify design limit behavior of current inelastic design provisions for compact bridges and extend the inelastic procedures to include noncompact designs.

The specific objectives of this paper are to (*a*) present the design and modeling of the test girder, (*b*) illustrate

the inelastic behavior, and (*c*) develop critical moment-inelastic rotation relations for the first test girder.

Inelastic Design of Steel Girder Bridges

ALFD inelastic design procedures (*1*) specify requirements at service load levels (normal traffic), overload levels (occasional heavy vehicle), and maximum load levels (one-time maximum vehicle). Inelastic LRFD provisions (2) specify these limits as Service I, Service II, and Strength I, respectively. The LRFD procedures also have a separate fatigue limit loading. Following are the LRFD load levels at the respective limits:

$$\text{Fatigue} = D + 0.75L(1 + I), \quad (1a)$$

$$\text{Service I} = D + 1.00L(1 + I), \quad (1b)$$

$$\text{Service II} = D + 1.30L(1 + I), \text{ and} \quad (1c)$$

$$\text{Strength I} = 1.25DC + 1.50DW + 1.75L(1 + I) \quad (1d)$$

where

D = dead load,
L = live load with lateral distribution factor,
I = impact factor (33 percent),
DC = component dead load (slab, beam, and barrier curbs), and
DW = wearing surface.

Fatigue and Service I limits are for fatigue and deflection checks. For inelastic design at the Service II limit state, after interior pier elastic moments are redistributed to adjacent positive moment regions, the design requirement is a limited stress at positive moment regions. At the Strength I level, a mechanism must not form with the application of the factored loads.

Prototype Bridge Design

The three-span two-lane protype bridge (18.3 × 23.2 × 18.3 m) (60 × 76 × 60 ft) was designed according to the fourth draft of the LRFD bridge design specifications using the inelastic design provisions (*2*). Four W30 × 108 rolled beam girders with 25.4-mm (1-in.) headed studs at a nominal spacing of 305 mm (12 in.) were selected. A girder spacing of 3.05 m (10 ft) was used to support the roadway that was 11.0 m (36 ft) wide. Yield strength of the steel was 345 MPa (50 ksi). The deck was 203 mm (8 in.) thick with 27.6 MPa (4,000 psi) compressive strength concrete and Grade 60 reinforcing steel. A future wearing surface of 0.57 kN/m^2 (12 psf) [about 25 mm (1 in.) of asphalt] and a barrier rail weighing 4.45 kN/m (305 plf) [a standard 406 mm (16 in.) concrete barrier curb] were considered as composite dead load. The bridge was designed assuming unshored construction. Also, the LRFD HS20 design vehicle and a lane load of 9.34 kN/m (64 plf) was used for determining live load effects. The 1/2-scale experimental test girder models an interior girder from the bridge system. Following is a brief description of the Service II and Strength I limit design procedures (*6*).

Elastic Analysis Techniques

A prismatic elastic analysis was used to compute the noncomposite dead load moments, and elastic nonprismatic analyses were used to determine the composite dead load moments and the live load plus impact moment envelopes. LRFD lateral distribution factors were used to approximate the amount of live load applied to a single girder. Figure 1 shows the total live and dead load moment envelopes for the prototype girder including impact and distribution factors.

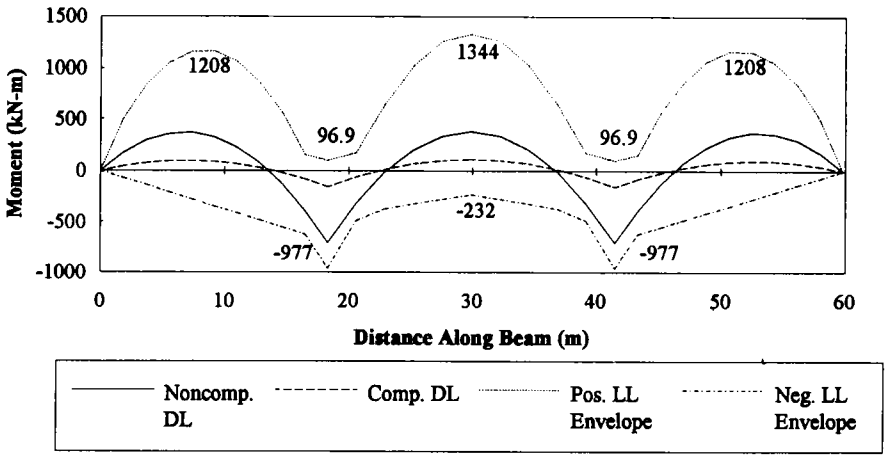

FIGURE 1 Prototype girder moment envelopes.

Design Limit States

Service II Limit State

The Service II check ensures that occasional overload vehicles equal to $1.30L(1 + I)$ will not cause excessive deformations. Elastic overload moments at the piers are shifted through residual moments, M_R, that occur at the pier because of inelastic pier rotations, θ_P. The residual moment is the difference between the elastic moment and the actual moment at the pier section. Due to inelastic action, the girder develops a residual moment field (self-equilibrating) that is locked in the structure and adds to other applied moments. The pier sections resist bending according to the following relationship (2).

$$M = M_P[0.7 - 60.0(\theta_P)] \leq 1.0 \tag{2}$$

where $-0.008 \leq \theta_P \leq 0$ radians,
M = actual moment in accordance with continuity and moment-rotation behavior,
θ_P = plastic rotation at pier in radians (negative), and
M_P = section plastic moment capacity.

For this design, residual moments were related to the pier rotation by an inelastic conjugate beam analysis developed by Dishongh (7). The moments at the piers caused by inelastic rotations at the piers, M_a and M_b, and the residual moment, M_R, are

$$M_a = \frac{\dfrac{EI\theta_P}{L}}{\left[\dfrac{-A}{3} - \dfrac{1}{2} + \dfrac{\dfrac{B}{6} + \dfrac{1}{4}}{B + 1}\right]} \tag{3a}$$

$$M_b = \frac{-M_a}{2B + 2} \tag{3b}$$

$$M_R = M_a + M_b \tag{3c}$$

where A and B are ratios of the two outer-span lengths to the center-span length 18.3/23.2 = 0.79.

At the pier section, the applied Service II moment, $[D + 1.30L(1 + I)]$ (Equation 1*c*), plus the residual moment (Equation 3*c*) is equal to the actual moment defined by the moment rotation relation (Equation 2) for composite pier sections:

$$[D + 1.30\,L(1 + I)] + M_R = M_P[0.7 - 60(\theta_P)] \tag{4}$$

Solving Equation 4 for the plastic rotation at the pier section yields $\theta_P = -0.00083$ radians. The residual moment was found as $M_R = 46$ kN-m (34 kip-ft) at the two-pier sections and throughout the middle span. The residual moment field is symmetric because of the symmetric bridge design.

For the Service II criteria, center-span, centerline stresses were found to be maximum. LRFD states that the applied stresses must be less than or equal to 0.95 of the flange yield stress, F_y, for composite, homogeneous sections in positive bending. The maximum Service II stress is determined by superposition of stresses where the live load moment stress component is equal to the elastic moment plus the redistributed residual moment. The total stress was calculated as 330 MPa (47.9 ksi), which is approximately equal to the requirement of $0.95\,F_y$ = 327 MPa (47.5 ksi).

Strength I Limit State

To satisfy the ultimate strength requirement, a plastic collapse mechanism must not form with the application of Strength I factored loads. LRFD inelastic provisions use an effective plastic moment, M_{PE}, at the negative moment pier hinge sections. The effective plastic moment accounts for moment unloading at large inelastic rotations. The mechanism check was carried out by applying the factored dead loads $[1.25DC + 1.50DW]$, moving the factored design truck $[1.75L(1 + I)]$ over the entire beam in tenth-point increments, and calculating the plastic collapse load factors for all truck positions (5). The critical mechanism, using M_{PE} at the pier sections, was the maximum positive center span loading configuration. The plastic collapse load factor was found to be 1.38: the structure can withstand 38 percent more factored live loads than caused by the Strength I factored design live loads. Thus, Strength I requirements did not control the design.

Test Girder Model

Structural modeling techniques were employed to determine the theoretical scale factors, S, for the ½-scale fundamental measures of interest. Steel and concrete properties for the prototype and the model were identical; therefore, the independent variables were chosen as elastic modulus, E (S_E = 1), and length, L (S_L = 2). The three-span test girder (18.3 × 23.3 × 18.3 m) (30 × 38 × 30 ft) was modeled to obtain near-equal width-thickness ratios and stresses. A W14 × 26 rolled shape with headed studs 12.7 mm (½ in.) at a nominal spacing of 152 mm (6 in.) was selected. The deck was 102 mm (4 in.) thick and 1.3 m (50.5 in.) wide with No. 3 rebar

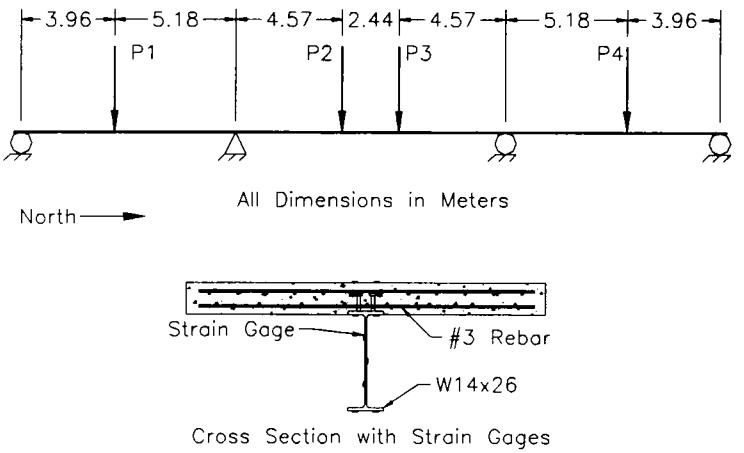

FIGURE 2 Model beam load locations and cross section.

in two layers in each direction. Figure 2 illustrates the test girder configuration.

Loading applied to the model was scaled to simulate equal stresses in the model and the prototype. Although most properties modeled closely, the scale factors for all the section moduli were approximately 8.5 instead of the theoretical 8.0. Therefore, to model equal stresses, all prototype bending moments were factored by 1/8.5.

Compensatory dead load was added to accurately simulate dead load stresses because a half-scale model weighs only one-quarter of the prototype and the proper scale factor is one-half. Ten concrete blocks 8.9 kN (2,000 lb) were hung from the bottom of the W-shape before the concrete deck was placed to compensate for the self-weight lost as a result of scaling. Additional concrete blocks were placed on top of the deck after it hardened to represent the composite dead loads (wearing surface, guard rails, etc.).

Moving live loads were simulated with four discrete loading points on the test beam, as indicated in Figure 2. Influence lines and linear programming were used to determine the sequence of loads needed to simulate a moving truck. Five individual load stages were developed to represent the moving load sequence. The critical location moments produced by the four discrete loading points are shown in Figure 3 along with the scaled Service I theoretical design truck [$L(1 + I)$] moment envelopes. The truck load sequence could be linearly adjusted to represent any percentage of the modeled truck design weight (LL).

Several different measurements were recorded for the test including rotation, deflection, reaction, strain

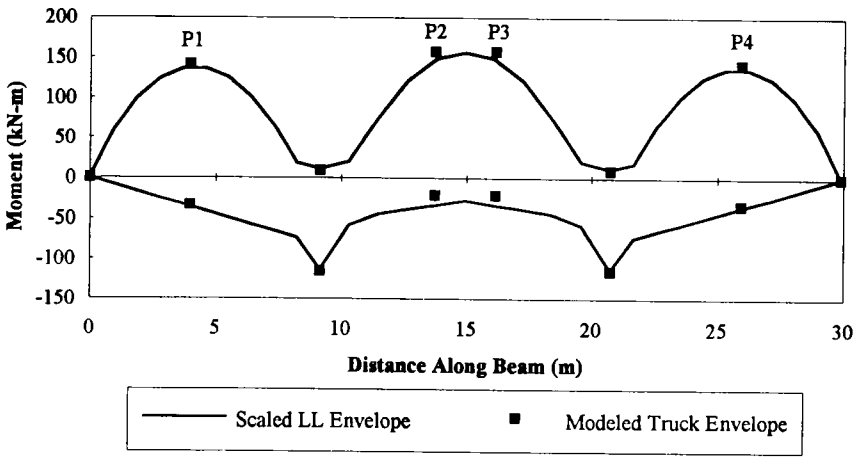

FIGURE 3 Modeled truck moment envelope and scaled prototype moment envelope.

gauge, and deck slip readings. The locations of these measurements are shown in Figure 4.

Testing and Design Limits

The modeled live loads were applied to the test beam at various load levels cyclically at slow rates (impact included in static load). The entire loading history of the test is as follows. Elastic low-level tests were carried out at 10, 20,40, 60, 70, 80, and 90 percent LL where LL is the modeled Service I loading. These provided an opportunity to confirm elastic behavior and instrumentation performance.

Service I level loads (100 percent LL) were applied to validate fatigue (ratioed to 75 percent LL) and deflection requirements of the LRFD provisions. Maximum strains at the fatigue level loading were 158 $\mu\epsilon$, whereas the LRFD limit is 200 $\mu\epsilon$. The maximum Service I elastic deflection was 31 mm (1.22 in.), which corresponds to a predicted deflection of 30 mm (1.16 in.). However, there was also a permanent set residual deflection of 3 mm (0.12 in.) at this level because of nonlinear behavior.

Increasing the loads toward the Service II level, loads of 110 and 120 percent LL were applied to examine the behavior in this range of loads. At the Service II level (130 percent LL), the girder experienced significant nonlinear behavior. Design provisions predict this residual deflection and limit stresses in positive moment portions of the structure to 0.95 Fy for composite girders. A maximum strain of 1450 $\mu\epsilon$ occurred at the bridge centerline compared with the allowed strain of 1638 $\mu\epsilon$ for 345 MPa (50 ksi) steel. Therefore, the structure met the Service II limit state criteria. However, at the 130 percent LL level, strain measurements in the negative bending sections were substantially higher than were elastic strains, indicating that some yielding had occurred in accordance with the design provisions. The residual deflection at the bridge centerline was 9.7 mm (0.38 in.) after the 130 percent LL loadings. The design provisions suggest cambering this residual deflection during fabrication.

Cyclic loads were applied at 140, 155, and 166 percent LL to examine the inelastic behavior above the Service II level. The last simulated moving load test was at 175 percent LL plus factored dead loads [$1.25DC + 1.5DW + 1.75L(1 + I)$] (Strength I level). This loading represents the worst possible maximum design load level applied to a bridge. The girder resisted this repeated load three times before some web buckling occurred. The final residual deflection from the moving load tests was 65 mm (2.6 in.).

After the cyclic tests, the girder was tested to failure by monotonically increasing loads proportioned to represent the theoretical design collapse configuration. This configuration simulated a stationary truck where the center axle of the truck was located at the centerline of the middle span. The additional factored dead load was applied by adding extra simulated loads to the P1 through P4 discrete load locations. Live loads were then applied to P1, P2, and P3 to recreate the prototype mechanism moment diagram. The P1 and P4 loads were set to load control for the duration of the collapse test, whereas the P2 and P3 loads were slowly increased under stroke control until the girder failed by concrete crushing at the bridge centerline. The maximum collapse load was 36 percent above the Strength I design limit. This corresponds to 38 percent excess capacity predicted in the design calculations.

Inelastic Behavior

Moving Load Tests

Each modeled truck weight percentage loading was repeated until the residual deflections stabilized and the bridge experienced shakedown. Figure 5 shows the permanent set residual deflection at the centerline of the bridge in terms of the percent Service I load level. This shakedown plot shows how the structure suffered increasing permanent set as the live load level increased. The onset of permanent set occurred at 70 percent LL. After the last cycle of loads, the girder had a residual deflection at the centerline of 65 mm (2.6 in.).

Stabilization of residual deflections was obtained with all live load levels except for the factored dead load plus 175 percent LL level (Strength I). Three cycles were carried out at the Strength I load level upon which each cycle resulted in large increases in residual deflection. The cyclic live loading portion of the test concluded at this level because some slight web buckling at the pier sections was detected. At the Strength I load level, the structure may or may not have shaken down. However, it can be concluded that the incremental collapse load, where inelastic deflections continually grow, occurred above the 166 percent LL level.

The moment-inelastic rotation at the negative moment pier section is the determining relation for the inelastic design method. From this behavior, the inelastic rotation, residual moment field, actual moments, and residual deflection are determined.

For the Service II limit, Figure 6 shows the moving load experimental moment-total rotation (elastic + inelastic) and the moment-inelastic rotation for the south pier. Figure 7 shows the same information except with the addition of the plastic collapse test moment-rotation data. Figure 6 includes live load negative moment loadings, whereas Figure 7 includes both dead and live load

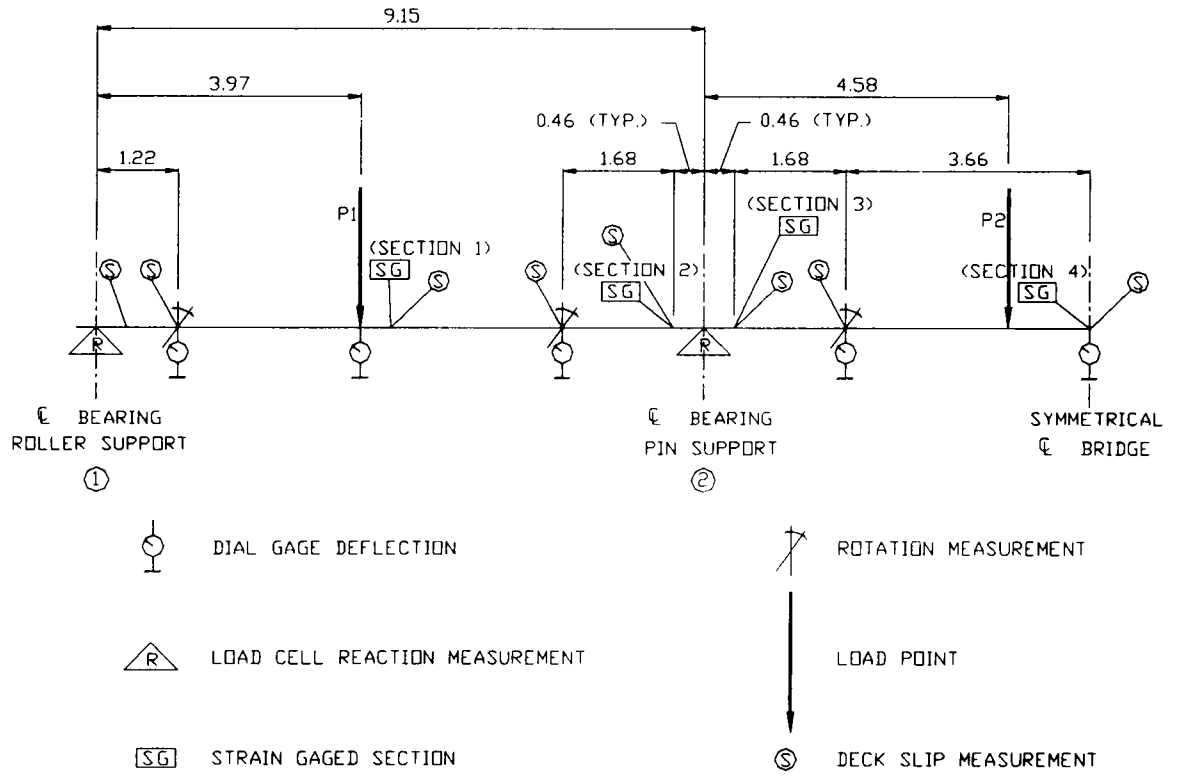

FIGURE 4 Measurement and load locations.

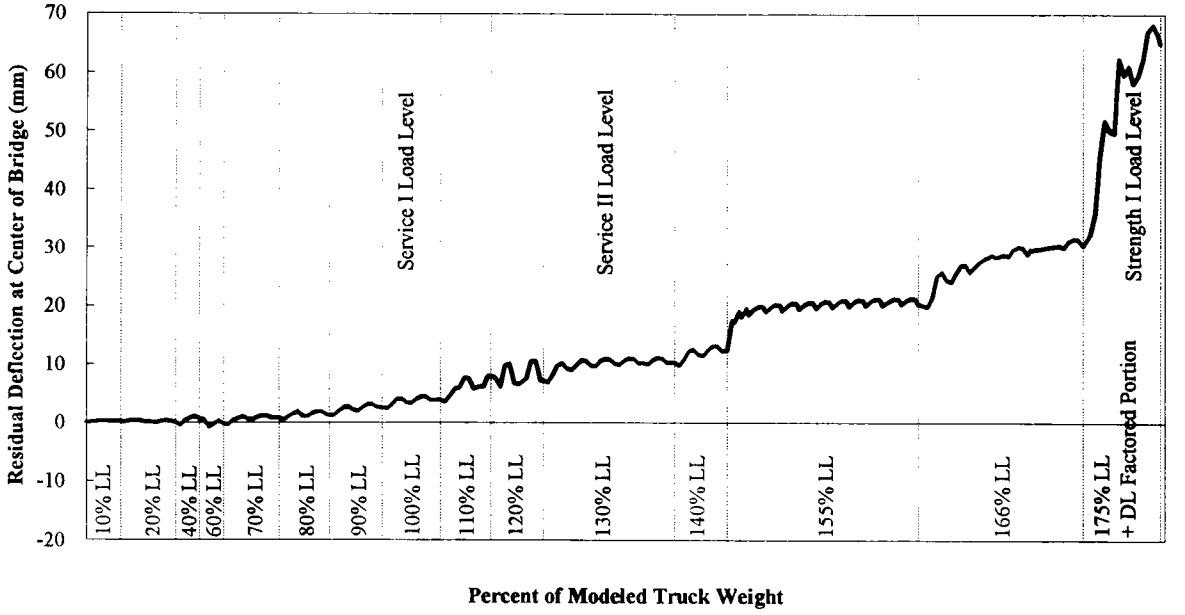

FIGURE 5 Residual deflection versus percent of modeled truck weight.

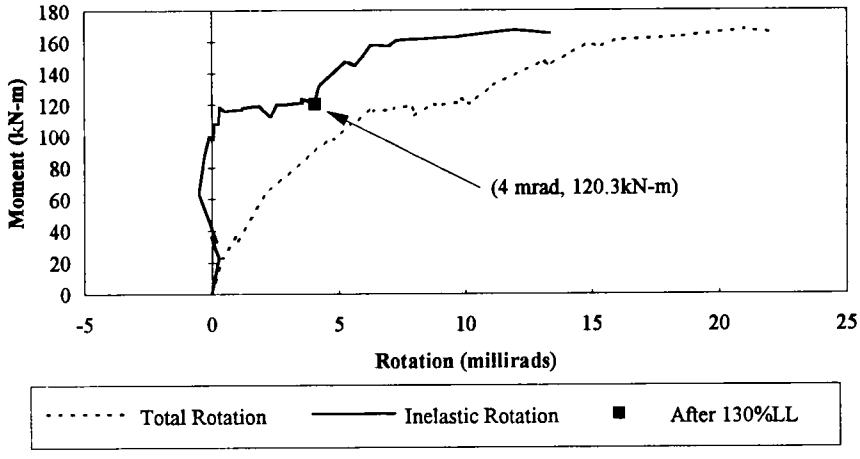

FIGURE 6 Negative moment: rotation for moving load test at pier.

negative moment loadings. From Figure 6, the inelastic rotation at the south pier (and north) is 4 mrad at the Service II level (130 percent LL).

Positive moment regions also show similar moment-rotation behavior, as shown in Figure 8 for the centerline of the girder. At the Service II level, the inelastic rotation is 0.8 mrad. Even though stresses are less than 0.95 Fy, there is some nonlinear behavior. The inelastic design provisions do not explicitly incorporate positive region inelastic rotation; however, although it is small, this inelastic rotation does have an effect on residual moments and deflections.

The residual deflection at 130 percent LL (design limit), based on the actual inelastic rotations at the two piers and at the girder centerline, is calculated in Figure 9. The conjugate beam method, using a length weighted moment of inertia, is employed loaded with an unknown residual moment field and known concentrated inelastic rotations. Figure 9 shows the calculated residual deflection to be 9.1 mm (0.36 in.), which is very close to the experimental deflection of 9.7 mm (0.38 in.). The determinate residual moment is 22 kN-m (16.2 kip-ft), which also agrees with experimental pier residual moments of 27.4 kN-m (20.2 kip-ft) and 25.9 kN-m (19.1 kip-ft) after the 130 percent LL load cycles.

The residual moment field increases the total moment in positive moment regions by adding to the elastic applied moments. Because this total moment must not cause stresses above 0.9 Fy, it is important to estimate the residual moment accurately. Thus, the pier section moment-rotation relation should represent the true behavior.

Concrete cracking over the pier regions, although important for serviceability, has little effect at Service I or Service II levels, as indicated in Figure 10. At low loads, the concrete is uncracked or partially cracked and the neutral axis is high in the beam. However, at design limit loads, the concrete has cracked sufficiently such

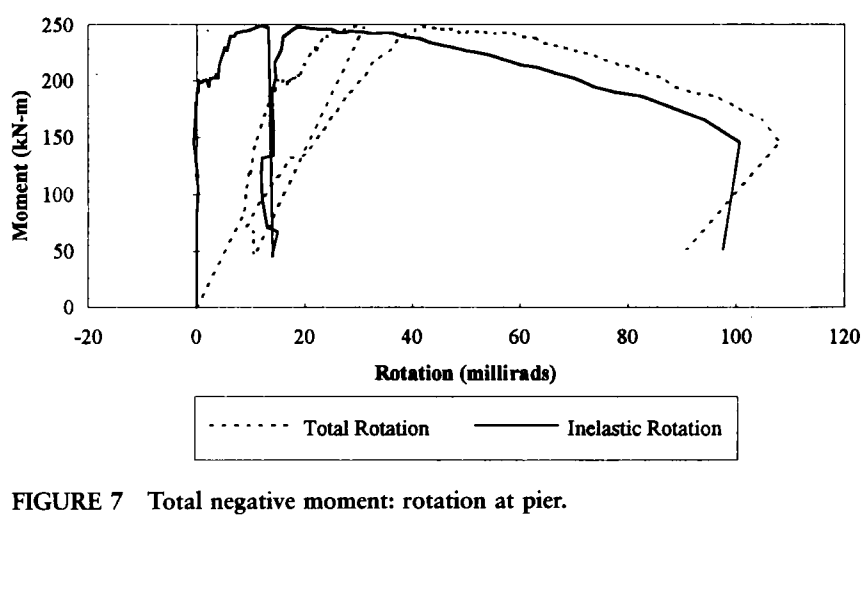

FIGURE 7 Total negative moment: rotation at pier.

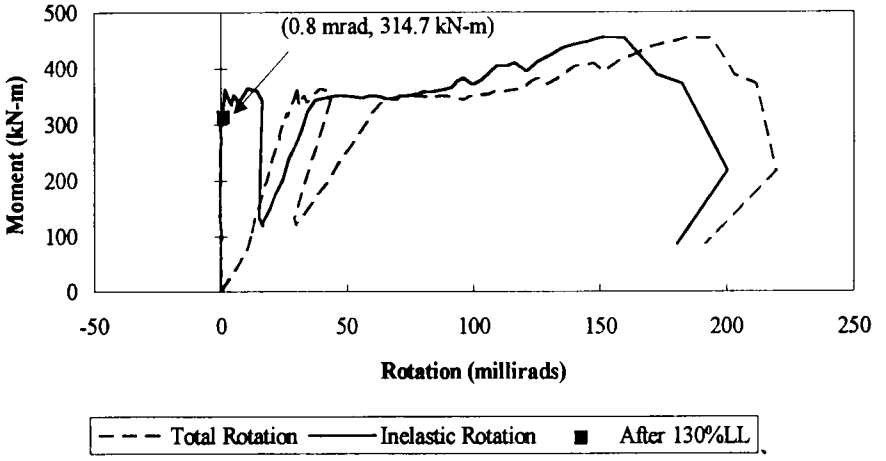

FIGURE 8 Total positive moment: rotation at bridge centerline.

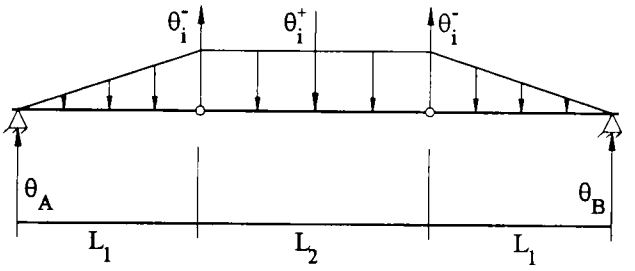

$$\theta_A = \theta_B = \frac{M_R L_1}{6EI}, \qquad \frac{M_R}{EI} = \frac{6\theta_i^- - 3\theta_i^+}{3L_2 + 2L_1}, \qquad \Delta_{CL} = \frac{\theta_i^- L_2}{2} - \frac{M_R L_2}{48EI}(6L_2 + 8L_1)$$

$$\theta_i^- = 4\,\text{mrads}, \theta_i^+ = 0.8\,\text{mrads}, E = 200\text{GPa and } I = 270\text{x}10^6\,\text{mm}^4$$

$$\Delta_{CL} = 9.1\text{mm}(0.36")$$

$$M_R = 22.0\text{kN} - \text{m}(16.2\text{k} - \text{ft})$$

FIGURE 9 Conjugate beam derivation.

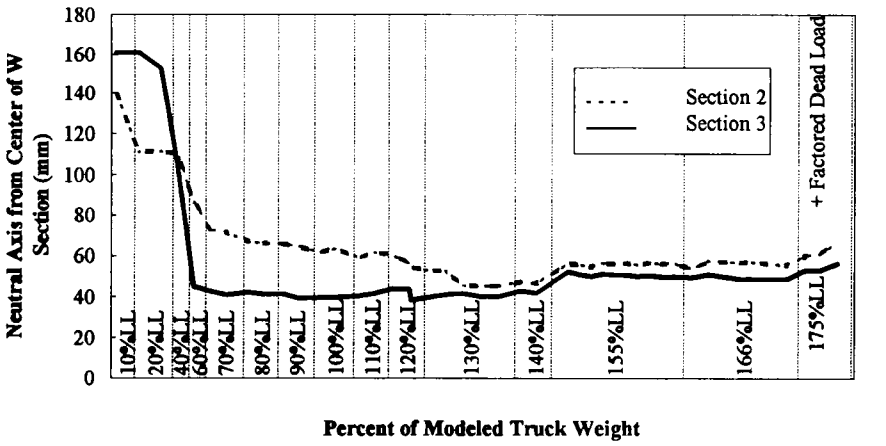

FIGURE 10 Section neutral axis location at pier for moving load test.

that the neutral axis has settled near the design position. At the 175 percent LL, the neutral axis starts to migrate toward the plastic hinge location.

Plastic Collapse Test

After the moving load tests, the girder was tested to failure by monotonically increasing loads proportioned to represent the theoretical design collapse configuration. The simulated factored portion of the dead load was applied to P1, P2, P3, and P4 and then P1, P2, and P3 were loaded to simulate the truck. Figure 11 is the total load at P2 and P3 (P2 + P3) plotted against the deflection at the girder centerline. The figure shows the Strength I factored load level (175 percent LL plus factored dead load) in relation to the load-deflection response. The figure clearly shows that the girder had excess capacity (36 percent) beyond the Strength I loading in accordance with the design calculations. The theoretical plastic collapse load was calculated using the effective plastic moment at the pier sections and the plastic moment capacity of the section at location P2. The actual maximum attained load was within 1 percent of the theoretical collapse load.

After sustaining about 356 mm (14 in.) of deflection at the bridge centerline (in addition to the 65 mm (2.6 in.) from the shakedown tests), the concrete crushed at the bridge centerline. Two aspects of the collapse test are worthy to note. The first is that the girder resisted 350 mm (13.8 in.) of deflection at near maximum loads. This deflection (length/deflection = 33) shows tremendous ductility for this compact girder. The second item is that this ductility behavior was not from an ideal elastic-perfectly plastic mechanism.

In Figure 7 it was seen that the pier sections are unloading moment with increasing rotation throughout the test. This is primarily caused by flange buckling, web buckling (started during the moving load tests), and lateral buckling. The lateral torsional buckling was very apparent with two distinct sine waves [sweep approximately 25 mm (1 in.)] between the bracing 1.22 m (4 ft) on each side of the pier. The flange and web buckling were visible but seemed to stabilize early in the collapse loading.

Although the pier sections were unloading, the centerline positive moment section was absorbing the redistributed moments as shown in Figure 8. The combination resulted in a very ductile girder.

Summary and Conclusions

More economical steel bridge designs (for compact girders) can be realized using inelastic design provisions. Inelastic design provisions can reduce material and fabrication costs by eliminating flange transitions and cover plates at interior piers (*5*). Bridge safety is not compromised because, after the structure has experienced several passes of the design limit loads, future loads are resisted elastically. Results from this test validate the LRFD inelastic provisions at all design limit states. Extending provisions to allow inelastic design for bridges comprising noncompact sections would also be beneficial. However, even though the analytical tools exist (*6*) for developing inelastic design procedures for these girders, large-scale testing is necessary to validate theoretical engineering practice.

The test results reported herein give an overview of the inelastic and plastic behavior of the ½-scale three-span composite test beam. The experimental results compared well with theoretical expectations. The test showed that residual deflections stabilize well above current serviceability limits. Also, the accuracy of pre-

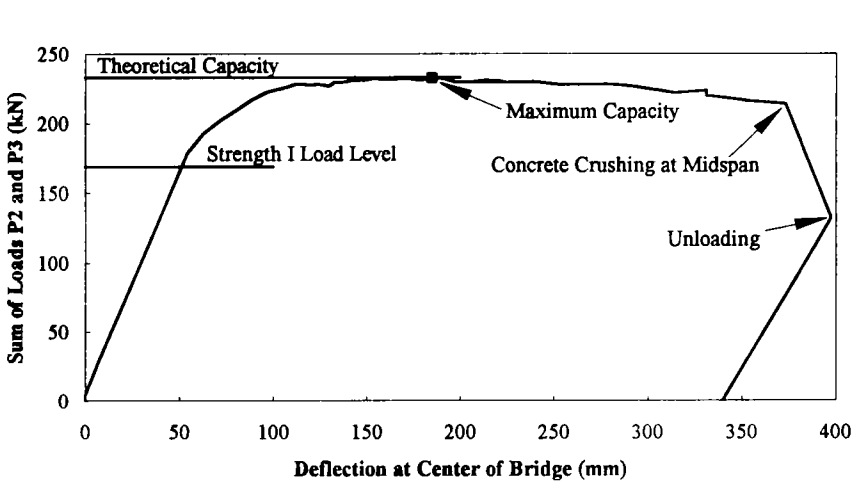

FIGURE 11 Collapse test middle span load: deflection response.

dicting inelastic behavior is dependent on the accuracy of the analytical models.

For inelastic design, estimating inelastic deflections, residual moments, and inelastic rotations is of great importance. The key to accurately predicting the bridge response is in the moment-inelastic rotation relation. This test produced one such relation for the negative pier region. However, it also developed the relation for positive bending. Positive inelastic rotations affect the results and can be easily incorporated into design provisions.

The plastic collapse test illustrated the ductility in compact composite beams. The primary reason that the beam behaved so well is that it is compact, with the flanges being well below the compactness requirements (ultracompact). This will not be the case for the second two girder tests planned for this project. The flanges will still be ultra-compact, but the webs will have typical plate girder width/thickness ratios. However, previous work has shown that, although these girders are not as ductile, the noncompact sections have predictable moment-rotation behavior (6) that can be incorporated into inelastic design provisions. The second two noncompact girder tests from this project will provide vital information for the development of inelastic design provisions for noncompact girders.

ACKNOWLEDGMENTS

The authors gratefully acknowledge the sponsors of this work: the National Science Foundation, the American Iron and Steel Institute, the American Institute for Steel Construction, the Missouri Highway and Transportation Department, Louisiana Transportation Research Center, Bethlehem Steel, Nucor-Yamato Steel, US Steel, St. Louis Screw & Bolt Co., and Stupp Bros. Inc.

REFERENCES

1. *Guide Specification for Alternate Load-Factor Design Procedures for Steel Beam Bridges Using Braced Compact Sections*. AASHTO, Washington, D.C., 1986.
2. *NCHRP Project 12-33: Load and Resistance Factor Design Bridge Design Specifications and Commentary*. Fourth Draft Copy. TRB, National Research Council, Washington, D.C., 1993.
3. Neal, B. G. *The Plastic Methods of Structural Analysis*, John Wiley & Sons, New York, 1956.
4. Barker, M. G. and T. V. Galambos, Shakedown Limit State of Compact Steel Girder Bridges, ASCE, *Journal of Structural Engineering*, Vol. 118, No. 4, April 1992, pp. 986–998.
5. Barker, M. G. Inelastic Design and Rating of Steel Girder Bridges. *Proc., 1993 National Symposium on Steel Bridge Construction*, Atlanta, Nov. 1993, pp. 2.1–2.17.
6. Weber, D. C. *Experimental Verification of Inelastic Load and Resistance Factor Design Limits*. Master's thesis. University of Missouri, Columbia, Aug. 1994.
7. Dishongh, B. E. *Residual Damage Analysis: A Method for the Inelastic Rating of Steel Girder Bridges*, Ph.D. thesis. University of Minnesota, Minneapolis, June 1990.